Article:
Ruffell, Jonathan E., Farmer, Thomas J. orcid.org/0000-0002-1039-7684, MacQuarrie, Duncan J. orcid.org/0000-0003-2017-7076 et al. (1 more author) (2019) The autoxidation of alkenyl succinimides - Mimics for polyisobutenyl succinimide dispersants. Industrial and Engineering Chemistry Research. pp. 1-12. ISSN: 0888-5885

https://doi.org/10.1021/acs.iecr.9b02780

I&EC research
Industrial & Engineering Chemistry Research

Article

Cite This: Ind. Eng. Chem. Res. XXXX, XXX, XXX−XXX

pubs.acs.org/IECR

The Autoxidation of Alkenyl Succinimides—Mimics for Polyisobutenyl Succinimide Dispersants

Jonathan E. Ruffell, Thomas J. Farmer, Duncan J. Macquarrie, and Moray S. Stark*

Department of Chemistry, University of York, York, YO10 5DD, U.K.

Supporting Information

ABSTRACT: Short chain alkenyl succinimides (ASIs) were synthesized and used as high purity chemical models to investigate the autoxidative degradation at 170 °C of polyisobutenyl succinimide dispersants (PIBSIs), a significant additive in automotive engine lubricants. Degradation products were characterized by gas chromatography−electron ionization mass spectrometry and quantified by gas chromatography-flame ionization detection. The rate of autoxidation of ASIs in a model lubricant, squalane, was also investigated. Although this is a complex molecule containing many possible sites of radical attack, all of the autoxidation products identified result from attack at the double bond or the adjacent allylic hydrogen atoms, which indicates the controlling influence of the double bond in the degradation of alkenyl succinimides, and therefore of commercial polyisobutenyl succinimide dispersants. The observed site-selective cleavage of the ASI structure, and by analogy PIBSI dispersants, would yield products that both reduce dispersancy and promote the formation of insoluble products that could have a detrimental effect on lubricant performance.

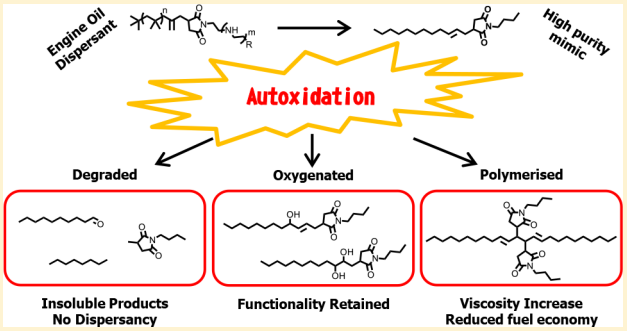

INTRODUCTION

Lubricants for modern internal combustion engines require a precisely formulated additive package to improve the performance of the lubricant and hence the engine; through cleaning, cooling, and protecting the engine, equipment lifetime and emissions can be improved. The harsh environment and high temperatures (115−180 °C) in an internal combustion engine can limit the lifetime of the lubricant through autoxidation.[1,2] Polar products of lubricant autoxidation can be insoluble in the relatively low polarity lubricant, the major component being a hydrocarbon based fluid. Polar products can impede lubricant flow, increasing mechanical wear and lubricant viscosity.[3] Higher viscosities increase friction which negatively impacts both fuel economy and greenhouse gas emissions.[4]

A fully formulated engine oil lubricant comprises an additive package and a viscosity index improver dissolved in a base oil; liquid hydrocarbons either produced synthetically or refined from crude oil. Constituting around 90% (w/w) of the lubricant oil, the mechanisms of base oil autoxidation have been investigated in detail through the use of model hydrocarbons.[5−11] Smaller hydrocarbons[12−15] and fatty acid methyl esters[16,17] have been investigated to determine fuel degradation mechanisms and higher mass ester base oils[18,19] used for lubricant degradation studies. More recently, focus has shifted to the impact of lubricant degradation on friction and wear performance, such as the degradation of molybdenum[20,21] or zinc based friction modifiers.[22,23] However, studies on lubricant additive autoxidation mechanisms, are limited. Beyond antioxidant studies, there has been little research in this area.[24,25] The effect of autoxidation on polyisobutenyl succinimide (PIBSI) dispersants is reported here.

Dispersants are amphiphilic additives that typically constitute between 4 and 8% (w/w) of an engine oil lubricant.[26] They solubilize polar products of lubricant degradation, known as sludge, and soot from the incomplete combustion of fuel.[4] Without dispersants, polar contaminants agglomerate, increasing friction and wear which reduces fuel efficiency and component lifetime.[27,28] PIBSIs (Figure 1) have been the main dispersant used since their development in the 1960s.[26] The commercial synthesis of PIBSI dispersants involves the Alder-ene addition of maleic anhydride (MAH) to the terminal alkene of oligomeric polyisobutene (PIB, Mw = 1000−2500 Da) which yields polyisobutenyl succinic anhydrides (PIBSAs).[26] Upon reaction with an amine, PIBSAs form the

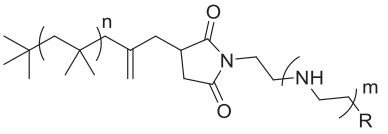

Figure 1. Idealized structure of a polyisobutenyl succinimide dispersant: *n* is typically 16−60, *m* is typically 3, and R = NH_2 or PIBSI.

Received: May 21, 2019
Revised: September 12, 2019
Accepted: September 19, 2019
Published: September 19, 2019

DOI: 10.1021/acs.iecr.9b02780
Ind. Eng. Chem. Res. XXXX, XXX, XXX−XXX

succinimide via the corresponding amic-acid.[29] Typically, ethyleneamines such as tetraethylenepentamine (TEPA) are used as the hydrophile. Using hydrophiles containing multiple primary amines allows *bis*-PIBSIs to be generated, with two PIB tails attached to a single hydrophile, altering the performance characteristics.[26]

Commercial dispersants have a general functionality but can have a very wide range of structures due to polyisobutene (PIB) polydispersity, ethyleneamine type and purity, and process variables. The characterization of PIBSI dispersants and their autoxidation products would be challenging and linking a degradation product to a specific starting molecule would be prohibitively complex, and therefore the chemical mechanisms by which they degrade would be very difficult to infer from product studies.

Therefore, alkenyl succinimides (ASIs) have been synthesized and used as high purity, single isomer, chemical models for PIBSI dispersants to elucidate the autoxidative breakdown mechanisms that could be applicable to commercial PIBSI dispersants. Succinimides are a complex structure, containing multiple potential sites for hydrogen abstraction and oxidation; however, the autoxidative behavior of succinimides under internal combustion engine conditions is unknown. In PIBSI dispersants, the alkene is located β to the succinimide group and so ASIs containing an alkene-β-succinimide moiety analogous to structures found in PIBSI dispersants were investigated (Figure 2). Their high purity and low molecular

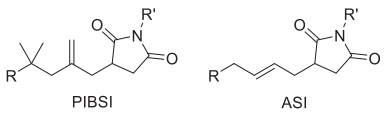

Figure 2. A comparison between the structures of PIBSI dispersants and ASI model dispersants.

weight (<400 Da) make ASIs and their autoxidation products suitable for analysis by gas chromatography (GC) coupled to mass spectrometry (MS) for characterization and flame ionization detection (FID) for quantification.

ASIs containing a low molecular weight PIB-like tail and an equivalent alkene-β-succinimide moiety cannot be synthesized from readily available starting materials. In this study, a readily producible alternative containing an *n*-alkyl tail was used. The ASI used contains secondary carbons, and PIBSIs contain primary, secondary, and quaternary carbons. As autoxidation is initiated by hydrogen abstraction, quaternary carbons would not be mechanistically important. Likewise, the high bond dissociation enthalpy of hydrogens located on primary carbons would limit their participation in autoxidation. Therefore, hydrogens located on secondary carbons in PIB would be the major site of autoxidative degradation of the hydrocarbon tail. As such, the secondary carbon containing ASI tail is reasoned to be of equivalent reactivity. However, this reasoning does not account for steric effects or relative rates of breakdown by β scission. ASIs containing a simple *n*-alkyl headgroup were used, opposed to ASIs with an aminic hydrophile. This was done to further simplify the system to focus on the degradation of the alkene-β-succinimide while avoiding ASI insolubility issues. A detailed study is reported here of the autoxidation of ASI dispersant mimics, with major products identified and quantified, and formation mechanisms discussed.

EXPERIMENTAL SECTION

A summary table of all experiments and analysis conducted can be found in the Supporting Information.

ASI Synthesis. A flask was charged with (2-dodecenyl)-succinic anhydride (4.00 g, 15 mmol) and heated to 60 °C under a flow of nitrogen. An *n*-alkyl amine was added (1.1 equiv), and the resultant mixture heated to 130 °C for 24 h with stirring under a flow of nitrogen. The crude product was purified by flash column chromatography on silica gel using 20% ethyl acetate in petroleum spirit (40−60 °C). ASI dispersant analogues were prepared with *n*-propyl, *n*-butyl, *n*-pentyl, *n*-hexyl, and *n*-heptyl amines yielding the corresponding *N*-alkyl ASI. Clear and colorless liquids were afforded for all *N*-alkyl ASIs in good yields and at least 98% purity as determined by gas chromatography with flame ionization detection (GC-FID). The purified product was characterized by proton nuclear magnetic resonance spectroscopy (^{1}H NMR), gas chromatography with electron ionization mass spectrometry (GC-EI-MS), and electrospray ionization mass spectrometry (ESI-MS) (see Supporting Information).

ASI Hydrogenation. A flask was charged with *N*-butyl ASI (4.0 g), 1% Pd on carbon (0.39 g, 0.3% (mol/mol) Pd) and heptane (200 mL). The resultant mixture was placed under a hydrogen atmosphere and stirred for 48 h at room temperature. The crude product was filtered through Celite and purified by flash column chromatography on silica gel with 20% ethyl acetate in petroleum spirit (40−60 °C) affording a white solid in good yields with 98% purity. The purified product, H_2-*N*-butyl ASI, was characterized by ^{1}H NMR spectroscopy, GC−EI-MS, ESI-MS and GC-FID (see Supporting Information).

Neat ASI Autoxidation. A 125 cm^3 three-necked round-bottom flask was heated to 170 °C under a flow of oxygen (0.04 L min^{-1}). The ASI (3.0 g) was added and held at 170 °C for 180 min with stirring. The liquid temperature was monitored using a K-type thermocouple. Samples (0.15 g) were taken at regular intervals and analyzed by GC-FID and GC−EI-MS. A schematic of the reaction set up can be found in the Supporting Information.

ASI Autoxidation in Squalane. A stainless steel (EN BS 304) reactor with a 55 cm^3 internal volume was heated to 170 °C under a flow of oxygen (0.04 L min^{-1}). A sample of ASI dissolved in squalane (10 cm^3, 5% w/w) was injected via a cannula. The temperature of the sample reached equilibrium in under 2 min, during which time autoxidation was assumed to be negligible. The mixture was held at 170 °C for 90 min with stirring (375 rpm). The liquid temperature was measured using a K-type thermocouple. Samples (0.3 mL) were taken at regular intervals and analyzed by quantitative GC-FID.[11] A schematic of the reaction set up can be found in the Supporting Information. Aging experiments were conducted in triplicate and analyzed once by GC-FID from which average values were calculated.

GC-FID. The concentrations of ASIs, squalane, and their autoxidation products were determined using a Shimadzu GC-17-A with a Phenomenex ZB-5HT column (30 m × 0.25 mm × 0.25 μm). Samples were not derivatized prior to quantitation. For all GC-FID samples, the accurately weighed sample (0.1 g to 4 significant digits) was dissolved in ethyl acetate (1.000 cm^3) to achieve an appropriate sample viscosity and concentration. The diluted sample was injected (1 μL) into the inlet held at 370 °C. Product **12** was quantified using a

DOI: 10.1021/acs.iecr.9b02780
Ind. Eng. Chem. Res. XXXX, XXX, XXX−XXX

2:1 split ratio with an initial oven temperature of 50 °C for 1 min with a 5 °C min^{-1} ramp to 340 °C which was held for 41 min. All other species were quantified using a 10:1 split ratio which allowed quantification of products representing >0.05% of the amount reacted material. The oven had an initial oven temperature of 50 °C for 1 min with a 5 °C min^{-1} ramp to 340 °C and hold for 10 min. Products of neat *N*-butyl ASI autoxidation were quantified using external calibration by the effective carbon number method.[31,32] For compounds for which authentic standards could not be obtained, FID response factors were estimated based on the structure of the analyte and an external calibration. A calibration curve of carbon number versus response factor for several pure alkanes from decane (carbon number 10) through to pristane (carbon number 19) was constructed. From this, response factors could be estimated based on calculated carbon number for a given analyte. The concentrations of *N*-butyl ASI and squalane were determined by external calibration using authentic standards.

ESI-MS. The sample (~1 mg) was dissolved in ethyl acetate (1 cm^3) and an aliquot (0.1 cm^3) was diluted further in methanol (1 cm^3) and injected (1 μL) in to an Agilent 1260 infinity liquid chromatograph with a 50:50 methanol/water mobile phase. The analyte was detected using a Bruker Compact time of flight mass spectrometer with internal calibration using sodium formate between m/z 90 and 1178. Resolution was ~12600 with mass errors <3 ppm as reported in the Supporting Information.

Unit Mass GC−EI-MS. Samples were analyzed using a PerkinElmer Clarus 500 gas chromatograph using a Restek Rxi-5HT column (30 m × 0.25 mm × 0.25 μm) coupled with a Clarus 500 quadrupole mass analyzer. The sample (100 mg) was dissolved in ethyl acetate (1 cm^3) and injected (1 μL) in to the inlet held at 50 °C. The GC oven had an initial temperature of 50 °C for 1 min with a 5 °C min^{-1} ramp to 340 °C which was held for 11 min. The EI source was held at 70 eV.

Accurate Mass GC−EI-MS. Samples were analyzed using an Agilent 7890 gas chromatograph using a Phenomenex ZB5-MS plus column (30 m × 0.25 mm × 0.25 μm) coupled to a Waters GTC Premier time of flight (ToF) mass analyzer. The sample (5 mg) was dissolved in ethyl acetate (1 cm^3) and injected (1 μL) into the inlet held at 50 °C. The oven had an initial temperature of 50 °C for 1 min with a 5 °C min^{-1} ramp to 340 °C which was held for 11 min. The electron ionization (EI) source was held at 70 eV. Samples were analyzed at both a 20:1 and a 2:1 split ratio to give good resolution of both high and low concentration analytes, respectively. The ToF mass analyzer was calibrated to authentic mass standards and an accurate mass defect was calculated relative to these standards and is reported in ppm. The root mean squared error of the mass analyzer was 10 ppm (see Supporting Information).

GC−MS Sample Derivatization. Silylation was used to functionalize the hydroxyl group containing species and identify structural isomers.[33−35] The sample (100 mg) was stirred in ethyl acetate (1 cm^3) with *N,O*-bis(trimethylsilyl) trifluoroacetamide/1% trimethylsilyl chloride (500 μL) at 50 °C for 3 h before being injected in to the GC−EI-MS, following the same analysis conditions used for nonderivatized samples.

Acetonide derivatization was used to functionalize vicinal diol containing species.[36,37] The sample (100 mg) was stirred in anhydrous acetone (5 cm^3) with anhydrous $CuSO_4$ (500 mg) at 50 °C for 3 h. The sample was filtered and concentrated under a flow of nitrogen before being injected in to the GC−EI-MS, following the same analysis conditions used for nonderivatized samples.

Compounds that did not contain hydroxyl functionality were characterized from samples prior to derivatization, and so their structures were unaffected by the heat, solvent, and reagents used in the derivatization steps.

NMR Spectroscopy. ^{1}H NMR spectra were recorded in $CDCl_3$ using a Jeol ECS 400 MHz spectrometer at 25 °C. Chemical shifts were calculated relative to $CHCl_3$.

Rheometry. Samples of *N*-butyl ASI before and after bulk phase autoxidation at 170 °C for 3 h were analyzed using a Brookfield R/S plus cone and plate rheometer at 20 °C using C50-1 and C25-2 spindles for low and high viscosity samples, respectively, with data recorded every second and smoothed using a 10-point moving average.

RESULTS

ASI Autoxidation Products. *N*-butyl ASI (Figure 3, R = *n*-butyl) was the main dispersant analogue studied for this work because of its favorable GC retention time as it did not overlap with the model base oil (squalane) or squalane autoxidation products. This allowed its concentration to be accurately monitored. In total, 15 products were identified using GC−EI-MS and quantified using GC-FID. Figure 4 shows a GC-FID chromatogram resulting from the liquid phase autoxidation of neat *N*-butyl ASI at 170 °C for 30 min from which 12 products have been characterized. A series of degradation products (**1**−**9**) with a significantly lower retention time than *N*-butyl ASI were observed. These result from the cleavage of C−C bonds in the ASI structure. A cluster of four peaks and a single peak (**10** and **11**, Figure 5) with a higher retention time than *N*-butyl ASI were characterized as oxygenated ASI products. These products contain the complete *N*-butyl ASI carbon skeleton with increased functionality through the addition of oxygen. A comparatively broad peak (**12**) was observed with a significantly higher retention time than the starting material. It was characterized as a dehydrodimer of *N*-butyl ASI, where two molecules of *N*-butyl ASI have dimerized by a recombination reaction, eliminating two hydrogen atoms and forming a covalent bond. As shown by Figure 6 and Figure 7, when *N*-butyl ASI was oxidized for a longer time (t > 60 min), two further degradation products (**13** and **14**) and a third oxygenated ASI product (**15**) were also observed.

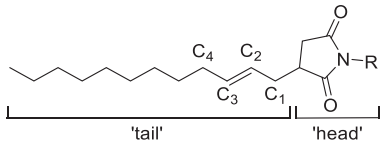

Figure 3. Labeling system for ASIs, R = *n*-propyl to *n*-heptyl.

To aid product assignment, a series of dispersant analogues with varying *N*-alkyl chain lengths (*n*-propyl to *n*-heptyl) were prepared and oxidized under the same conditions. Figure 8 shows the GC-FID traces of *N*-propyl to *N*-heptyl ASIs oxidized for 30 min at 170 °C. ASIs were prepared with the same C_{12} "tail" and therefore fragment species with the same retention times (**1**, **2**, **3**, **6**, and **7**) contained the ASI "tail" but not the *N*-alkyl chain from the "head" group. Species originating from the succinimide "head" group (**4***, **5***, **8***,

DOI: 10.1021/acs.iecr.9b02780
Ind. Eng. Chem. Res. XXXX, XXX, XXX−XXX

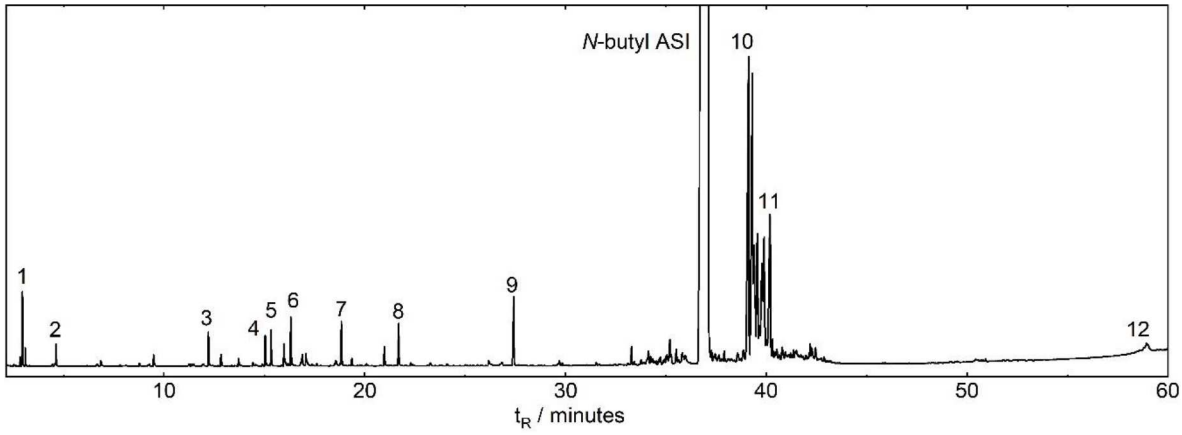

Figure 4. A GC-FID chromatogram of oxidized *N*-butyl ASI (autoxidation at 170 °C for 30 min) showing degradation products (**1**–**9**), unreacted *N*-butyl ASI, oxygenated ASI products **10** and **11**, and the *N*-butyl ASI dehydrodimer (**12**).

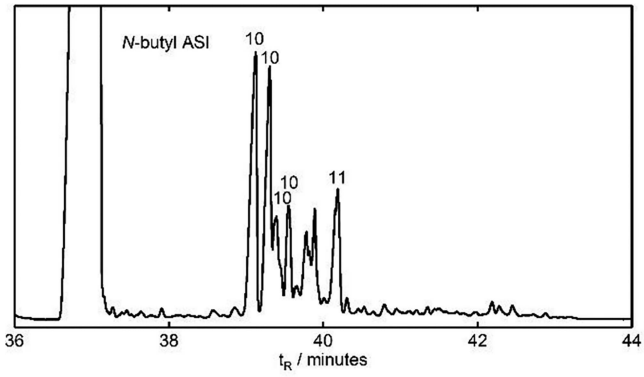

Figure 5. An expansion of the GC-FID chromatogram in Figure 4.

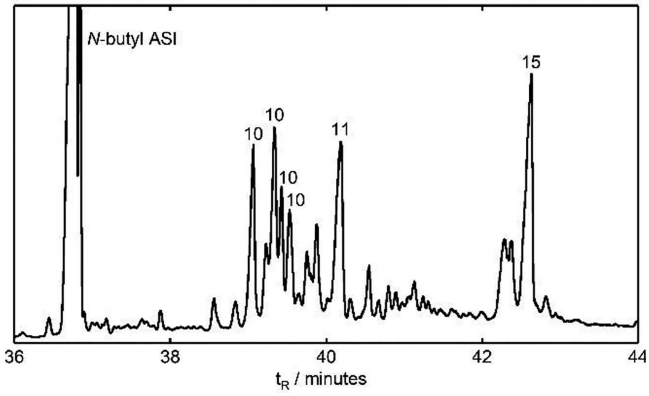

Figure 7. An expansion of the GC-FID chromatogram in Figure 6 showing unreacted *N*-butyl ASI and oxygenated ASI products **10**, **11**, and **15**.

and **9***) showed progressively longer retention times with longer *N*-alkyl chains. The retention times of all functionalized ASI products increased with increasing *N*-alkyl chain length.

Fifteen products of *N*-butyl ASI autoxidation at 170 °C were characterized by accurate mass GC–EI-MS. Table 1 gives the structures identified. Regioisomers of functionalized ASI products and their formation mechanisms are discussed with respect to the numbering in Figure 3. The EI spectra of fragments originating solely from the "tail" of *N*-butyl ASI (**1**, **2**, **3**, **6**, **7**, and **13**) were readily characterized by reference to the NIST database. Originating from the ASI "head", *N*-butyl succinimide (**4**) was also characterized in this way. Where NIST database matches could not be found (**5**, **8**, **9**, **10**, **11**, **12**, **14**, and **15**) accurate mass measurements were used to determine chemical formulas and fragment ions were used to determine structure. Silylation and acetonide derivatization were used to confirm the presence of hydroxyl groups and identify regioisomers. Assignments are reported and discussed in the Supporting Information.

Product Distribution. Autoxidation products of *N*-butyl ASI were quantified by GC-FID from samples taken during the

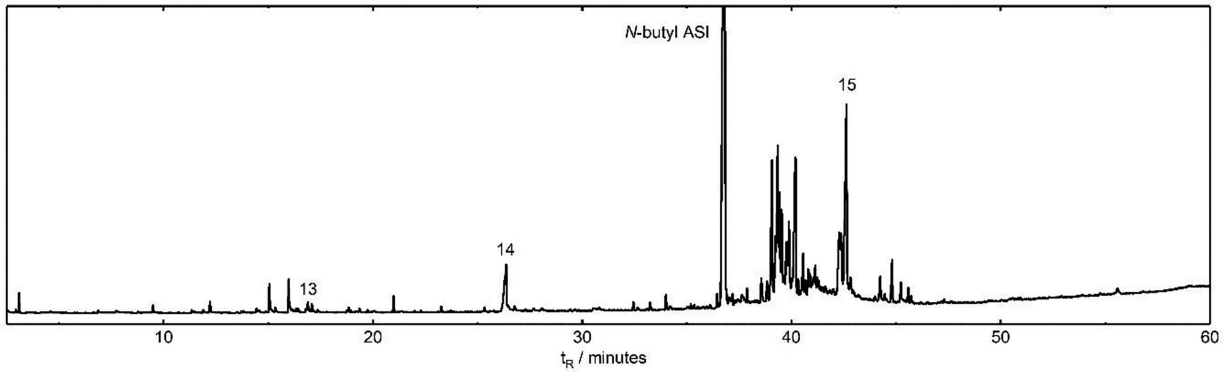

Figure 6. A GC-FID chromatogram of oxidized *N*-butyl ASI (autoxidation at 170 °C for 180 min) showing degradation products **13** and **14**, unreacted *N*-butyl ASI and oxygenated ASI product **15**.

DOI: 10.1021/acs.iecr.9b02780
Ind. Eng. Chem. Res. XXXX, XXX, XXX–XXX

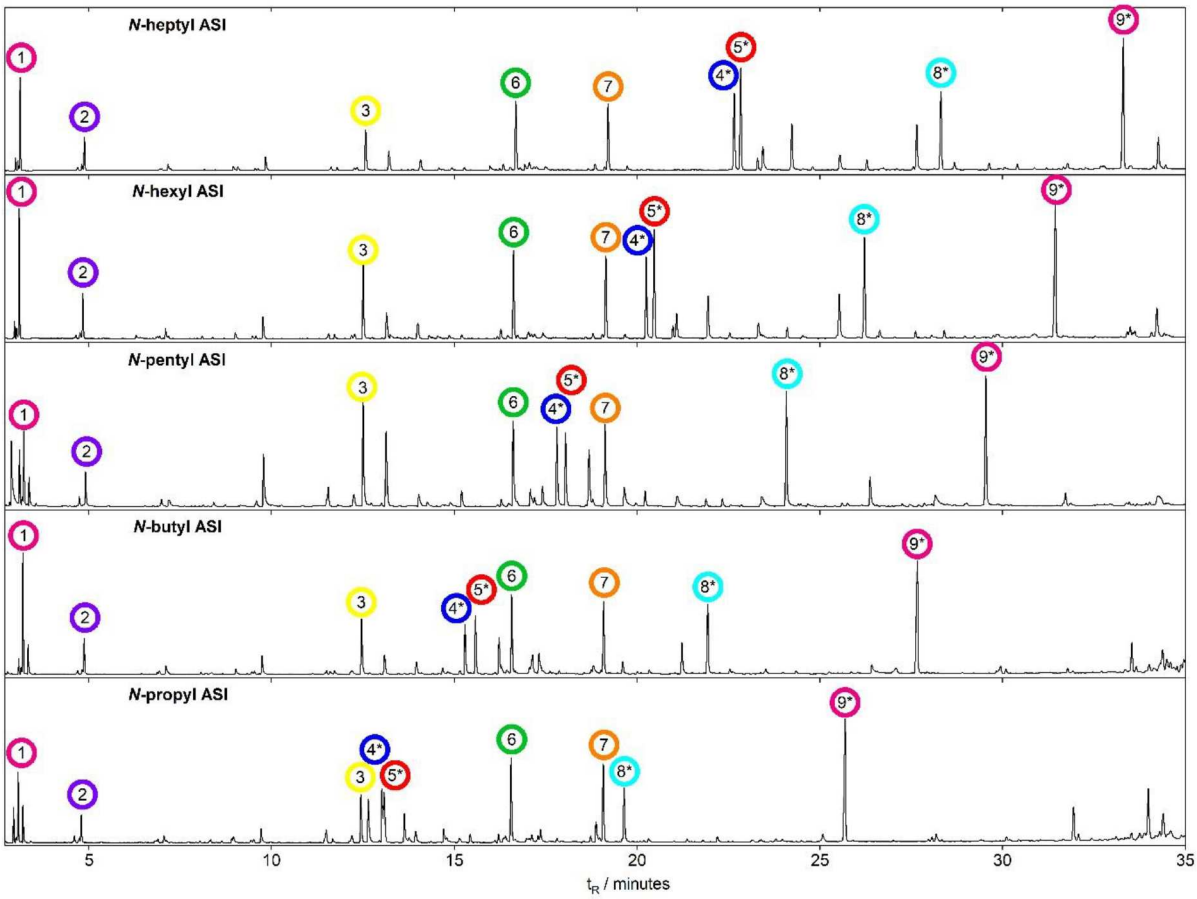

Figure 8. GC-FID chromatograms of oxidized ASIs (*N*-propyl to *N*-heptyl, 170 °C, 30 min) between 0 and 35 min. Species with equivalent retention times (**1**, **2**, **3**, **6**, and **7**) originate from the ASI "tail". Species originating from the succinimide "head" group (**4***, **5***, **8***, and **9***) show increasing retention time with increasing *N*-alkyl chain lengths.

3 h reaction. The quantification of individual fragment products and the dehydrodimer can be found in the Supporting Information and the concentrations of functionalized ASI products are shown in Figure 9. While the *N*-butyl ASI alcohol (**10**) and *N*-butyl ASI ketone (**11**) concentrations increased from t_0, the C_2,C_3 *N*-butyl ASI diol (**15**) was only observed after 60 min. The concentration of the *N*-butyl ASI alcohol (**10**) decreased after 90 min.

Reaction selectivities were also calculated, defined as the proportion of reacted material that goes on to form a certain product or group of products. The data from one experiment is given in Figure 10. The selectivity was calculated for the sum of the ASI degradation products, with GC retention times lower than *N*-butyl ASI, and for the sum of the oxygenated ASI products, the products observed with GC retention times higher than *N*-butyl ASI. As the structures of all observed peaks had not been determined, molar concentrations could not readily be calculated, so, selectivity was calculated based on the GC-FID peak areas for all observed peaks. Early in the reaction (5 min), the selectivity for *N*-butyl ASI forming degradation products was 17%, decreasing to 4% over the first 60 min. The selectivity for oxygenated ASI products increased from 27% early in the reaction to a maximum of 36% after 50 min, after which it decreased to a low of 24% by the end of the reaction.

At the start of the reaction, the liquid sample contained pure *N*-butyl ASI which was also monitored by GC-FID. As the reaction progressed, the sum of the peak areas for *N*-butyl ASI and all the observed products noticeably decreased, with a selectivity for products that were observable by GC-FID of 44% early in the reaction (at 5 min), decreasing to 27% by the end of the 3 h reaction. This is attributed to the formation of higher molecular weight and higher polarity species that are not detectable due to their very low volatility at the maximum GC temperature used (340 °C).

Viscosity Increase. The dynamic viscosity of *N*-butyl ASI before and after autoxidation at 170 °C for 3 h was measured at shear rates between 50 and 750 s^{-1}. Prior to autoxidation, *N*-butyl ASI showed Newtonian behavior with a low and shear-independent viscosity of 0.06 Pa s. After autoxidation, the sample viscosity at a shear rate of 50 s^{-1} was 17.6 Pa s, a 300-fold increase. The sample showed reversible shear thinning behavior with the viscosity decreasing to 14.4 Pa s when the shear rate was ramped to 750 s^{-1}. After a hold period of 5 min when no shear force was applied, the sample showed the same shear thinning behavior for a second and third shear cycle (Figure 11).

ASI Autoxidation in Squalane. The autoxidative stability of two ASIs in a lubricant oil mimic (squalane) was tested at 170 °C using a steel reactor with a continuous oxygen flow following a previously described procedure.[11] A control experiment of pure squalane oxidized under the same conditions was also conducted. The decay rate of both squalane and the ASI dispersant mimic was measured for 5% (w/w) solutions of either *N*-butyl ASI or H_2-*N*-butyl-ASI, its hydrogenated analogue, in squalane. The concentrations were

DOI: 10.1021/acs.iecr.9b02780
Ind. Eng. Chem. Res. XXXX, XXX, XXX−XXX

Table 1. Identified Products from the Autoxidation of *N*-Butyl ASI at 170 °C

Peak	Name	Structure
1[a]	octane	
2[a]	nonane	
3[a]	decanal	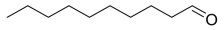
4[a]	*N*-butyl succinimide	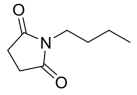
5[b]	3-methyl, *N*-butyl-succinimide	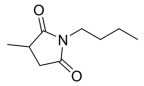
6[a]	undec-2-enal	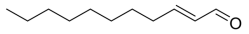
7[a]	dodec-2-enal	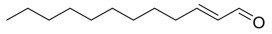
8[b]	succinimide aldehyde	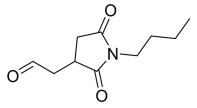
9[b]	α,β-unsaturated succinimide aldehyde	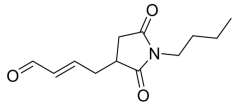
10[b,c]	*N*-butyl ASI alcohol e.g. C_4 *N*-butyl ASI alcohol	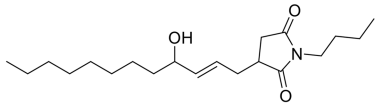
11[b]	C_4 *N*-butyl ASI ketone	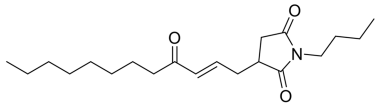
12[b]	*N*-butyl ASI dehydrodimer e.g. C_1-C_1 *N*-butyl ASI dehydrodimer	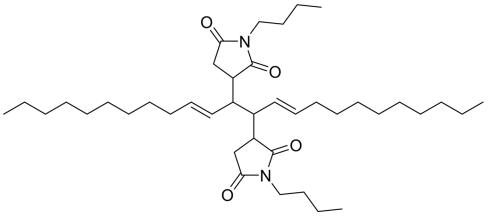
13[a]	n-decanoic acid	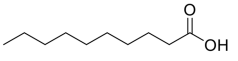
14[b,c]	succinimide acid	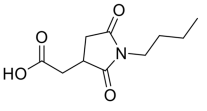
15[b,c,d]	C_2,C_3 *N*-butyl ASI diol	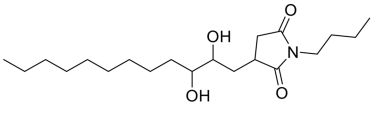

[a]Identified by comparison to the NIST database. [b]EI MS fragment assignments made and reported in the Supporting Information. [c]Silylated derivative observed. [d]Acetonide derivative observed.

DOI: 10.1021/acs.iecr.9b02780
Ind. Eng. Chem. Res. XXXX, XXX, XXX−XXX

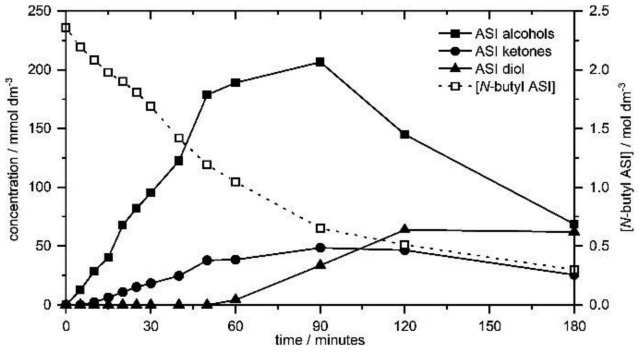

Figure 9. Concentration *N*-butyl ASI alcohols, (**10**), *N*-butyl ASI ketone (**11**), and the C_2,C_3 *N*-butyl ASI diol (**15**) during the autoxidation. The concentration of *N*-butyl ASI is also shown.

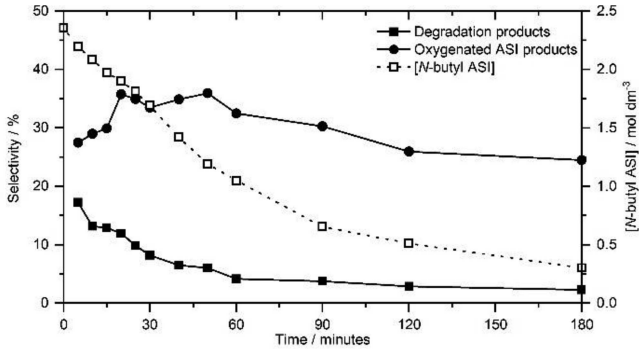

Figure 10. Selectivity for all observed degradation products and all observed oxygenated ASI products. The concentration of *N*-butyl ASI is also shown.

representative of dispersants in commercial lubricants.[4] The reactant concentrations were monitored by GC-FID, shown in Figure 12. By GC-FID, squalane and its degradation products did not coelute with the ASI peak allowing accurate monitoring of their concentration throughout the reaction. After an induction period of 15 min the decay of both ASIs and squalane was approximately first order; to quantify the rates of reaction, pseudo-first order rate constants were calculated (Table 2). Volatile species were condensed at 0 °C from the reactor exhaust gases and analyzed by GC-FID. Squalane and

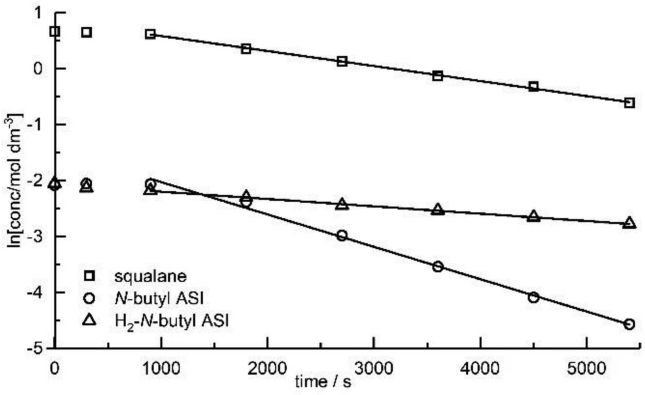

Figure 12. Natural logarithm of squalane, *N*-butyl ASI and H_2-*N*-butyl ASI concentrations during autoxidation at 170 °C. The data for squalane concentrations are from the autoxidation of squalane with no ASI present. Pseudo-first-order rate constants were calculated from the linear fit after the 15 min induction period.

Table 2. Pseudo-first-order Rate Constant of Squalane, *N*-Butyl ASI, and H_2-*N*-Butyl ASI Decay at 170 °C[a]

	pseudo-first-order rate constant/$10^{-4}s^{-1}$		
sample	squalane	*N*-butyl ASI	H_2-*N*-butyl ASI
squalane	2.79 ± 0.07		
5% (w/w) *N*-butyl ASI in squalane	2.69 ± 0.05	6.15 ± 0.10	
5% (w/w) H_2-*N*-butyl ASI in squalane	2.67 ± 0.07		1.31 ± 0.06

[a]Aging experiments were conducted in triplicate from which the average and standard error was calculated.

the ASIs were not observed and so losses of these molecules can be solely attributed to autoxidative breakdown, with no significant contribution from evaporative losses.

DISCUSSION

ASI Autoxidation Mechanisms. The products observed indicate ASI autoxidation mechanisms are comparable with those observed in hydrocarbon autoxidation[5−14] which is initiated by the abstraction of labile hydrogen atoms by molecular oxygen (reaction 1). The resultant carbon-centered

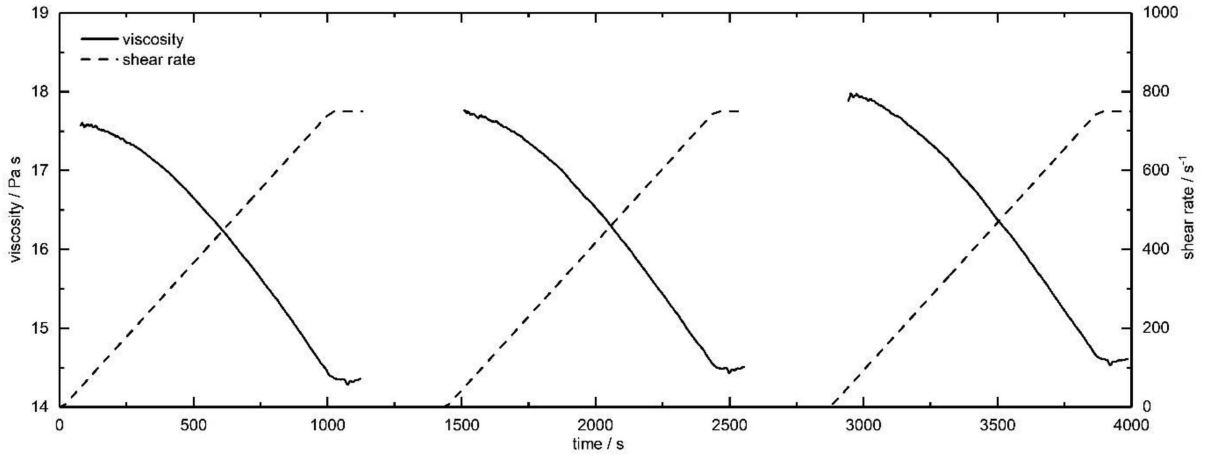

Figure 11. Dynamic viscosity behavior of *N*-butyl ASI after autoxidation at 170 °C for 3 h over three cycles with shear rates between 50 s^{-1} and 750 s^{-1}.

DOI: 10.1021/acs.iecr.9b02780
Ind. Eng. Chem. Res. XXXX, XXX, XXX−XXX

radicals (R•) can react with oxygen forming alkyl peroxyl radicals (reaction 2).[9] These abstract a hydrogen atom from another molecule to form alkyl peroxides and regenerating R• (reaction 3).[41]

$$\text{R-H} + \text{O}_2 \rightarrow \text{R}\cdot + \text{HO-O}\cdot \quad (1)$$

$$\text{R}\cdot + \text{O}_2 \rightarrow \text{R-O-O}\cdot \quad (2)$$

$$\text{R-O-O}\cdot + \text{R-H} \rightarrow \text{R-O-O-H} + \text{R}\cdot \quad (3)$$

The hydroperoxides formed by reaction 3 are the primary nonradical product of hydrocarbon autoxidation however, at the elevated temperatures used in this study, peroxides readily decompose forming hydroxyl and alkoxyl radicals (reaction 4).[42] Subsequent hydrogen abstraction by the resultant alkoxyl radicals forms alcohols (reaction 5) while regenerating alkyl radicals, continuing the autoxidation chain reaction.

$$\text{R-O-O-H} \rightarrow \text{R-O}\cdot + \cdot\text{OH} \quad (4)$$

$$\text{R-O}\cdot + \text{R-H} \rightarrow \text{R-O-H} + \text{R}\cdot \quad (5)$$

Products from Alkoxyl Radical Formation. Four isomers of the *N*-butyl ASI alcohol (**10**) were observed and fully characterized in this work. The alcohol within these structures was allylic in nature, positioned at either C_1, C_2, C_3, or C_4 (Figure 3). No other alcohol isomers were observed, showing autoxidation was initiated by highly specific abstraction of allylic hydrogens. This can be explained by the C−H bond dissociation enthalpy (BDE), whereby a lower BDE and higher stability of the formed radical give a higher rate of abstraction.[14,30,38] BDE and carbon-centered radical stability increase in the order primary < secondary < tertiary < allylic,[39] and so allylic alcohols were the major products observed. Allylic hydrogens at C_1 and C_4 (Figure 3) were the dominant site of hydrogen abstraction. After abstraction, the resultant radicals at C_1 and C_4 can shift spin density to the C_3 and C_2 positions, respectively, as previously observed for the autoxidation of monounsaturated lipids.[40] Hence, there are four radical sites to react further; C_1, C_2, C_3, and C_4. Via reactions 1, 2, 3 and 4, alkoxyl radicals are selectively formed at C_1, C_2, C_3, and C_4 sites. Hydrogen abstraction by alkoxyl radicals (reaction 5) forms the corresponding allylic alcohol, which is consistent with the four observed isomers of the *N*-butyl ASI alcohol (**10**). The C_4 *N*-butyl ASI ketone (**11**) can also form through alkoxyl radical intermediates.[11] Abstraction of hydrogen by molecular oxygen from an alkoxyl radical in the allylic C_4 position could form the ketone and a hydroperoxyl radical (reaction 6).

$$\text{HR}_2\text{C-O}\cdot + \text{O}_2 \rightarrow \text{R}_2\text{C=O} + \text{HO-O}\cdot \quad (6)$$

The C_4 *N*-butyl ASI ketone was the only ketone containing product characterized, however its GC peak (**11**) showed evidence for the coelution of multiple ketone isomers. From the *N*-butyl ASI alcohol (**10**), there is evidence for the formation of alkoxyl radicals at the C_1, C_2, C_3, and C_4 positions. All alkoxyl radical isomers could form the ketone and so the uncharacterized ketone products are likely C_1, C_2, and C_3 ketone isomers.

For the formation of degradation products, the major cleavage mechanism is thought to be α cleavage of alkoxyl radicals (reaction 7) and the products observed all resulted from alkoxyl radical formation at C_1, C_2, C_3, and C_4 sites.[10]

$$\text{HR}_2\text{C-O}\cdot \rightarrow \text{HRC=O} + \text{R}\cdot \quad (7)$$

The α cleavage of allylic alkoxyl radicals is preferential, cleaving the C−C bond β to the alkene to yield an α,β-unsaturated aldehyde and a comparatively stable alkyl radical, opposed to the less stable vinylic radical from cleavage of the bond α to the alkene (Scheme 1).[43]

Scheme 1. Preferential Cleavage of an α,β-Unsaturated Alkoxyl Radical

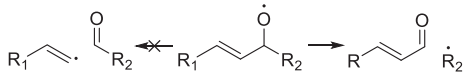

Hydrogen abstraction by the resultant alkyl radical fragment ($R_2\cdot$ in Scheme 1) to yield the corresponding alkane (reaction 8) accounts for the formation of octane (**1**), nonane (**2**), *N*-butyl succinimide (**4**), and 3-methyl, *N*-butyl-succinimide (**5**).

$$\text{R}_2\cdot + \text{R-H} \rightarrow \text{R}_2\text{-H} + \text{R}\cdot \quad (8)$$

The major primary fragment products observed arose from the α cleavage of C_1 to C_4 alkoxyl radicals; however, the α,β-unsaturated aldehyde fragment expected to form from α cleavage of a C_3 alkoxyl radical (Scheme 2) was not observed. The resultant succinimide fragment would contain a highly resonant stabilized tertiary carbon. The low C−H BDE would make this species highly reactive, and so it was not observed.

Hydroxyl Radical Addition to the Alkene. Neither decanal (**3**), succinimide aldehyde (**8**), or the C_2,C_3 *N*-butyl ASI diol (**15**) can be attributed to initial abstraction of allylic hydrogens. These degradation products represent cleavage across the ASI alkene, and the C_2,C_3 *N*-butyl ASI diol (**15**) represents reduction of the alkene and alcohol formation at C_2 and C_3. Their formation is consistent with direct hydroxyl radical (·OH) addition to the alkene. Upon addition of ·OH to the alkene, a carbon-centered radical is generated α to the newly formed alcohol (Scheme 3, reaction 9a). The addition of O_2 to the alkyl radical yields an α-hydroxy peroxyl radical (Scheme 3, reaction 9b). This species can abstract hydrogen (Scheme 3, reaction 9c) and upon homolysis of the resultant peroxide (Scheme 3, reaction 9d), an α-hydroxy alkoxyl radical is formed.[44]

By reaction 10, the α-hydroxy alkoxyl radical would yield decanal (**3**) and succinimide aldehyde (**8**).[45]

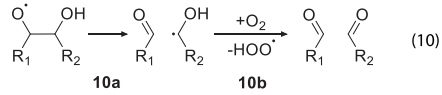

(10)

An alternative mechanism for aldehyde formation by •OH addition to alkenes is possible. The Waddington mechanism (reaction 11) involves the decay of the α-hydroxy peroxyl radical through a cyclic six-membered transition state. Simultaneous α cleavage eliminates a hydroxyl radical yielding two aldehydes.[46]

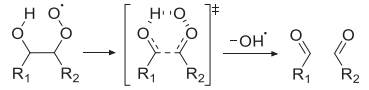

(11)

Conventional lubricant degradation mechanisms would suggest the formation of carboxylic acid degradation products as a major secondary oxidation product, formed via the further oxidation of highly reactive aldehydes, which in turn can oxidize to carboxylic acids.[11] In the later stages of *N*-butyl ASI oxidation, small concentrations of two carboxylic acids were identified, a carboxylic acid containing succinimide and *n*-

DOI: 10.1021/acs.iecr.9b02780
Ind. Eng. Chem. Res. XXXX, XXX, XXX−XXX

Scheme 2. Formation and Subsequent Degradation of the Expected Product of Alkoxyl Radical α Cleavage at the C_3 Position of *N*-Butyl ASI

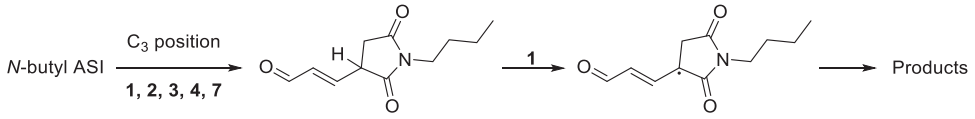

Scheme 3. Formation of an α-Hydroxy Alkoxyl Radical by Hydroxyl Radical Addition to an Alkene

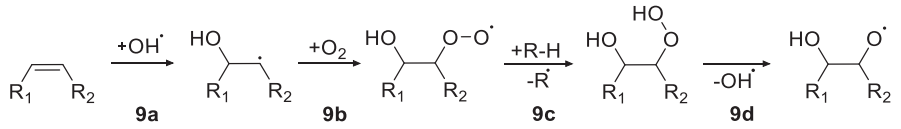

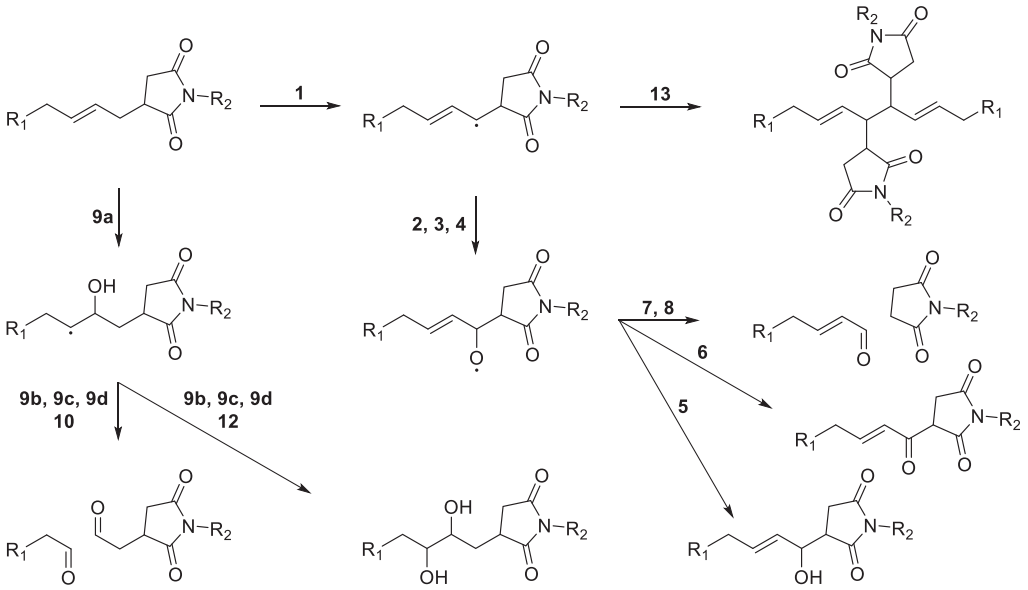

Figure 13. Mechanism for ASI autoxidation showing the three major routes to the 13 primary products identified in ASI autoxidation.

decanoic acid (peaks **13** and **14**, respectively), consistent with formation from the further oxidation of an aldehyde containing succinimide and decanal (peaks **3** and **8**, respectively, see Supporting Information for characterization).

The formation of the C_2,C_3 *N*-butyl ASI diol (**15**) can be accounted for by hydrogen abstraction by the α-hydroxy alkoxyl radical formed in Scheme 3 (reaction 12). When *N*-butyl ASI was oxidized, decanal (**3**) and succinimide aldehyde (**8**) were observed in the initial stages of the reaction, whereas the C_2,C_3 *N*-butyl ASI diol (**15**) was only observed after 60 min. Formation of the diol involves an intermolecular hydrogen abstraction, and therefore a source of sufficiently labile hydrogen atoms is required. The delayed formation of the C_2,C_3 *N*-butyl ASI diol (**15**) suggests the hydrogen donated to the α-hydroxy alkoxyl radical is unlikely to be donated by a second equivalent of *N*-butyl ASI. Instead, a source of sufficiently labile hydrogens must accumulate noticeably to compete with decay by fragmentation.

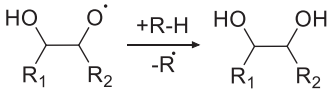

Recombination. The formation of the *N*-butyl ASI dehydrodimer (**12**) is attributed to recombination of two carbon-centered ASI radicals (reaction 12), a known radical termination mechanism.[47] Recombination of any of the four allylic radical isomers would yield 10 different dehydrodimer regioisomers which is consistent with the broad GC peak observed.

$$R_1\cdot + R_2\cdot \rightarrow R_1 - R_2 \qquad (13)$$

The reaction selectivity (Figure 10) suggested the formation of high molecular weight and high polarity species, unobservable by GC, to be a major radical termination route. However, the concentration of the *N*-butyl ASI dehydrodimer (**12**) plateaued at a low concentration early in the reaction suggesting it reacted further.

The tertiary hydrogens of the *N*-butyl ASI dehydrodimer (**12**) are highly labile, promoting rapid further oxidation of the *N*-butyl ASI dehydrodimer (**12**), yielding products of relatively high mass and polarity that are unobservable by GC.

This work has found significant evidence that the autoxidation of ASIs is highly specific, reacting only at allylic sites or at the alkene itself. The overall mechanism for the formation of the observed products of ASI autoxidation is shown in Figure 13. In summary, all of the observed autoxidation products can be accounted for by chemical mechanisms following from either hydroxyl radical addition to the double bond, or abstraction of the allylic hydrogen atoms adjacent to the double bond, thus demonstrating the controlling influence of the double bond in the degradation of alkenyl succinimides, and by extension, of commercial

DOI: 10.1021/acs.iecr.9b02780
Ind. Eng. Chem. Res. XXXX, XXX, XXX−XXX

polyisobutenyl succinimide dispersants. The succinimide group or the long alkane tail do not noticeably contribute to degradation.

Relative Reactivities. The reactivity of *N*-butyl ASI and its hydrogenated analogue, H_2-*N*-butyl ASI, was examined relative to a model base oil, squalane. Both squalane and ASIs followed first order decay when oxidized at 170 °C. Shown in Table 2, the pseudo-first-order rate constant for the decay of *N*-butyl ASI was 2.3 times higher than that of squalane. Studied by Stark et al., squalane primarily reacts by hydrogen abstraction at one of the six tertiary carbon sites,[11] whereas this work has shown ASIs preferentially react by abstraction of one of four hydrogens at allylic sites. Therefore, ASI allylic hydrogens are approximately 3.5 times more reactive at 170 °C than tertiary hydrogens in a model lubricant. This means, in a real lubricant, the dispersant will decay significantly quicker than the lubricant base oil.

By way of comparison, the induction period for liquid phase autoxidation of *n*-octane, which contains only primary and secondary hydrogen atoms, is approximately twice as long as for 2-methylpheptane (one tertiary as well as six secondary hydrogens),[14] which supports the suggestion that a comparatively low proportion of hydrogen atoms with a lower bond strength can have a noticeable effect on the rate of autoxidation of a molecule. To confirm the importance of the alkene in ASI autoxidation, the alkene of *N*-butyl ASI was hydrogenated. After hydrogenation, its decay rate constant was 4.7 times lower than *N*-butyl ASI showing the importance of the alkene for dispersant autoxidation, and that hydrogenation is an effective way to improve the oxidative stability of ASI dispersant mimics.

Viscosity Increase. The viscosity of *N*-butyl ASI increased 300-fold after oxidation at 170 °C for 3 h, suggesting the formation of high molecular weight and/or high polarity species. This viscosity increase is attributed to the *N*-butyl ASI dehydrodimer and its subsequent autoxidation products; higher polarity species and higher order polymers than the dehydrodimer that were not detectable by GC (Figure 10). The oxidized ASI also showed non-Newtonian behavior, whereby the viscosity decreased as shear force increased (Figure 11). This shear thinning was reversible; when the shear force was stopped for 5 min, the viscosity increased back to its original value. Reversibility suggests the shear thinning effect was due to breaking intermolecular bonds, such as hydrogen bonds between alcohol groups. Bonds are reformed as the shear force decreases, increasing the viscosity back to the original value. As well as high polarity species, high molecular weight products likely also contribute to the large viscosity increase upon ASI autoxidation.

Implications for PIBSI Dispersant Degradation during Use in Engine Lubricants. When the mechanisms of ASI autoxidation are applied to PIBSI dispersants, several significant performance impacts can be inferred. Dispersants are used to solubilize polar oxidation products derived from lubricant autoxidation, known as sludge, and soot from incomplete fuel combustion that would otherwise agglomerate within the lubricant. Soot and sludge formation alters the rheology of a fluid. Lubricants with high soot and sludge loading exhibit shear-thinning non-Newtonian behavior due to shear forces breaking up intermolecularly bonded agglomerates, like the observation made for oxidized *N*-butyl ASI. A PIBSIs amphiphilic structure allows soot and sludge dispersion which prevents agglomerates from forming. This not only gives Newtonian rheology but also mitigates the negative performance impacts of soot and sludge on mechanical wear and fuel economy.[27] The fragmentation of PIBSI dispersants via the α cleavage or OH radical addition mechanisms demonstrated in this work has severe performance implications.

Site-specific cleavage of the polar headgroup from the apolar tail would render the dispersant inactive. Not only does this reduce the concentration of active dispersant, but cleavage liberates the polar headgroup into the lubricant which, being insoluble in the lubricant base oil, would agglomerate and contribute to sludge formation. Therefore, fragmentation would have a significant and detrimental impact on both dispersant performance and lubricant rheology.

Recombination of radicals to yield the ASI dehydrodimer, and subsequent reactions to form heavier and more polar species, is suggested to be a significant oxidation pathway for ASI autoxidation and can account for the observed 300-fold viscosity increase at low shear rates.

In a lubricant oil, allylic carbon-centered radicals formed by hydrogen atom abstraction can also self-react to form the ASI dehydrodimer, or react with other carbon-centered radicals, formed, for example, by hydrogen abstraction from the base fluid molecules, to form heavier and often more polar species. This is suggested to be a significant oxidation pathway for bulk ASI oxidation, leading to a viscosity increase which can increase mechanical friction, decrease fuel economy, and increase CO_2 emissions.

The selectivity for the three major decay routes, recombination, oxygenation, and degradation, is likely to be dependent on the lubricant formulation. For instance, a source of labile hydrogens, such as a radical-scavenging antioxidant (AO), would donate hydrogen atoms to alkoxyl and carbon-centered PIBSI radicals, limiting their decay by α cleavage and recombination, respectively. Through its rapid degradation the addition of PIBSI dispersants to a lubricant increases its radical forming ability and therefore reducing its lifetime. Formulators can mitigate this by increasing the AO concentration; however, it comes at an additional cost.

CONCLUSIONS

Alkenyl succinimides (ASIs) have been studied as chemical models for the autoxidation of polyisobutenyl succinimide (PIBSI) dispersants. The initial radical attack was shown to be site specific, either by abstraction of resonance-stabilized allylic hydrogen atoms or hydroxyl radical addition to the alkene. Allylic ASI alcohols, ASI ketones, and seven degradation products were characterized and attributed to alkoxyl radical formation. The formation of an ASI diol is attributed to the initial addition of a hydroxyl radical to the alkene (reaction 9a in Figure 13) and subsequent reactions with oxygen, R-H and hydroxyl radical elimination to form a hydroxy-alkoxyl radical (reactions 9b, 9c, 9d in Figure 13), which can then abstract a hydrogen atom to form the diol (reaction 12 in Figure 13). Two aldehydes can also be accounted for by ·OH addition to the alkene followed by α cleavage of the hydroxy-alkoxyl radical (reaction 10 in Figure 13). The recombination of carbon-centered ASI radicals is thought to be a major product forming route with high molecular weight products contributing to a 300-fold viscosity increase. Allylic ASI hydrogens were found to be 3.5 times more reactive (at 170 °C) than tertiary hydrogens of squalane, a lubricant oil mimic. Degradation of PIBSI dispersants would negatively impact their dispersing

DOI: 10.1021/acs.iecr.9b02780
Ind. Eng. Chem. Res. XXXX, XXX, XXX−XXX

performance and PIBSI dehydrodimers would increase lubricant viscosity, harming fuel economy and CO_2 emissions.

■ ASSOCIATED CONTENT

Supporting Information

The Supporting Information is available free of charge on the ACS Publications website at DOI: 10.1021/acs.iecr.9b02780.

Summary of the analyses; product characterizations and identification; chromatograms; mass spectra (PDF)

■ AUTHOR INFORMATION

Corresponding Author

*E-mail: moray.stark@york.ac.uk.

ORCID

Thomas J. Farmer: 0000-0002-1039-7684

Duncan J. Macquarrie: 0000-0003-2017-7076

Moray S. Stark: 0000-0002-2175-2055

Notes

The authors declare no competing financial interest.

■ ACKNOWLEDGMENTS

The authors would like to thank Afton Chemical Ltd. for funding this research and Karl Heaton for conducting high resolution MS analysis.

■ REFERENCES

(1) Moritani, H.; Nozawa, Y. Oil Degradation in Second-Land Region of Gasoline Engine Pistons. *Rev. Toyota CRDL* **2004**, *38* (3), 36−43.

(2) Taylor, R. I.; Evans, P. G. In-Situ Piston Measurements. *Proc. Inst. Mech. Eng., Part J* **2004**, *218* (3), 185−200.

(3) Green, D. A.; Lewis, R. The Effects of Soot-Contaminated Engine Oil on Wear and Friction: A Review. *Proc. Inst. Mech. Eng., Part D* **2008**, *222* (9), 1669−1689.

(4) Atkinson, D.; Brown, A. J.; Jilbert, D.; Lamb, G. Formulation of Automotive Lubricants. In *Chemistry and Technology of Lubricants*; Mortier, R. M., Fox, M. F., Orszulik, S., Eds.; CRC Press: London, 2010; pp 293−324.

(5) Jalan, A.; Alecu, I. M.; Meana-Pañeda, R.; Aguilera-Iparraguirre, J.; Yang, K. R.; Merchant, S. S.; Truhlar, D. G.; Green, W. H. New Pathways for Formation of Acids and Carbonyl Products in Low-Temperature Oxidation: The Korcek Decomposition of γ-Ketohydroperoxides. *J. Am. Chem. Soc.* **2013**, *135* (30), 11100−11114.

(6) Blaine, S.; Savage, P. E. Reaction Pathways in Lubricant Degradation. 1. Analytical Characterization of n-Hexadecane Autoxidation Products. *Ind. Eng. Chem. Res.* **1991**, *30* (4), 792−798.

(7) Blaine, S.; Savage, P. E. Reaction Pathways in Lubricant Degradation. 2. n-Hexadecane Autoxidation. *Ind. Eng. Chem. Res.* **1991**, *30* (9), 2185−2191.

(8) Blaine, S.; Savage, P. E. Reaction Pathways in Lubricant Degradation. 3. Reaction Model for n-Hexadecane Autoxidation. *Ind. Eng. Chem. Res.* **1992**, *31* (1), 69−75.

(9) Jensen, R. K.; Korcek, S.; Mahoney, L. R.; Zinbo, M. Liquid-Phase Autoxidation of Organic Compounds at Elevated Temperatures. 1. The Stirred Flow Reactor Technique and Analysis of Primary Products from n-Hexadecane Autoxidation at 120−180.Degree.C. *J. Am. Chem. Soc.* **1979**, *101* (25), 7574−7584.

(10) Jensen, R. K.; Korcek, S.; Mahoney, L. R.; Zinbo, M. Liquid-Phase Autoxidation of Organic Compounds at Elevated Temperatures. 2. Kinetics and Mechanisms of the Formation of Cleavage Products in n-Hexadecane Autoxidation. *J. Am. Chem. Soc.* **1981**, *103* (7), 1742−1749.

(11) Stark, M. S.; Wilkinson, J. J.; Smith, J. R. L.; Alfadhl, A.; Pochopien, B. A. Autoxidation of Branched Alkanes in the Liquid Phase. *Ind. Eng. Chem. Res.* **2011**, *50* (2), 817−823.

(12) Mielczarek, D. C.; Matrat, M.; Amara, A. B.; Bouyou, Y.; Wund, P.; Starck, L. Toward the Accurate Prediction of Liquid Phase Oxidation of Aromatics: A Detailed Kinetic Mechanism for Toluene Autoxidation. *Energy Fuels* **2017**, *31* (11), 12893−12913.

(13) Chatelain, K.; Nicolle, A.; Ben Amara, A.; Catoire, L.; Starck, L. Wide Range Experimental and Kinetic Modeling Study of Chain Length Impact on N-Alkanes Autoxidation. *Energy Fuels* **2016**, *30* (2), 1294−1303.

(14) Chatelain, K.; Nicolle, A.; Ben Amara, A.; Starck, L.; Catoire, L. Structure−Reactivity Relationships in Fuel Stability: Experimental and Kinetic Modeling Study of Isoparaffin Autoxidation. *Energy Fuels* **2018**, *32* (9), 9415−9426.

(15) Ben Amara, A.; Nicolle, A.; Alves-Fortunato, M.; Jeuland, N. Toward Predictive Modeling of Petroleum and Biobased Fuel Stability: Kinetics of Methyl Oleate/n-Dodecane Autoxidation. *Energy Fuels* **2013**, *27* (10), 6125−6133.

(16) Dugmore, T. I. J.; Stark, M. S. Effect of Biodiesel on the Autoxidation of Lubricant Base Fluids. *Fuel* **2014**, *124*, 91−96.

(17) Frauscher, M.; Besser, C.; Allmaier, G.; Dörr, N. Elucidation of Oxidation and Degradation Products of Oxygen Containing Fuel Components by Combined Use of a Stable Isotopic Tracer and Mass Spectrometry. *Anal. Chim. Acta* **2017**, *993*, 47−54.

(18) Frauscher, M.; Besser, C.; Allmaier, G.; Dörr, N. Oxidation Products of Ester-Based Oils with and without Antioxidants Identified by Stable Isotope Labelling and Mass Spectrometry. *Appl. Sci.* **2017**, *7* (4), 396.

(19) Cen, H.; Morina, A.; Neville, A. Effect of Lubricant Ageing on Lubricants' Physical and Chemical Properties and Tribological Performance; Part I: Effect of Lubricant Chemistry. *Ind. Lubr. Tribol.* **2018**, *70* (2), 385−392.

(20) De Feo, M.; Minfray, C.; De Barros Bouchet, M. I.; Thiebaut, B.; Le Mogne, T.; Vacher, B.; Martin, J. M. Ageing Impact on Tribological Properties of MoDTC-Containing Base Oil. *Tribol. Int.* **2015**, *92*, 126−135.

(21) De Feo, M.; Minfray, C.; De Barros Bouchet, M. I.; Thiebaut, B.; Martin, J. M. MoDTC Friction Modifier Additive Degradation: Correlation between Tribological Performance and Chemical Changes. *RSC Adv.* **2015**, *5* (114), 93786−93796.

(22) Dörr, N.; Brenner, J.; Ristić, A.; Ronai, B.; Besser, C.; Pejaković, V.; Frauscher, M. Correlation Between Engine Oil Degradation, Tribochemistry, and Tribological Behavior with Focus on ZDDP Deterioration. *Tribol. Lett.* **2019**, *67* (2), 1−17.

(23) Dörr, N.; Agocs, A.; Besser, C.; Ristić, A.; Frauscher, M. Engine Oils in the Field: A Comprehensive Chemical Assessment of Engine Oil Degradation in a Passenger Car. *Tribol. Lett.* **2019**, *67* (3), 1−21.

(24) Alfahad, A. The Behaviour of Antioxidants in Automotive Engine Oils. Ph.D. Thesis, University of York, 2008.

(25) Jensen, R. K.; Korcek, S.; Zinbo, M.; Gerlock, J. L. Regeneration of Amine in Catalytic Inhibition of Oxidation. *J. Org. Chem.* **1995**, *60* (17), 5396−5400.

(26) Seddon, E. J.; Friend, C. L.; Roskki, J. P. Detergents and Dispersants. In *Chemistry and Technology of Lubricants*; Mortier, R. M., Fox, M. F., Orszulik, S. T., Eds.; Springer: Dordrecht, 2010; pp 213−237.

(27) Bagi, S.; Sharma, V.; Aswath, P. B. Role of Dispersant on Soot-Induced Wear in Cummins ISB Engine Test. *Carbon* **2018**, *136*, 395−408.

(28) Vyavhare, K.; Bagi, S.; Patel, M.; Aswath, P. B. Impact of Diesel Engine Oil Additives-Soot Interactions on Physiochemical, Oxidation, and Wear Characteristics of Soot. *Energy Fuels* **2019**, *33* (5), 4515−4530.

(29) Balzano, F.; Pucci, A.; Rausa, R.; Uccello-Barretta, G. Alder-Ene Addition of Maleic Anhydride to Polyisobutene: Nuclear Magnetic Resonance Evidence for an Unconventional Mechanism. *Polym. Int.* **2012**, *61* (8), 1256−1262.

(30) Pfaendtner, J.; Broadbelt, L. J. Mechanistic Modeling of Lubricant Degradation. 1. Structure−Reactivity Relationships for Free-Radical Oxidation. *Ind. Eng. Chem. Res.* **2008**, *47* (9), 2886−2896.

DOI: 10.1021/acs.iecr.9b02780
Ind. Eng. Chem. Res. XXXX, XXX, XXX−XXX

(31) Jorgensen, A. D.; Picel, K. C.; Stamoudis, V. C. Prediction of gas chromatography flame ionization detector response factors from molecular structures. *Anal. Chem.* **1990**, *62* (7), 683−689.
(32) Scanlon, J. T.; Willis, D. E. Calculation of Flame Ionization Detector Relative Response Factors Using the Effective Carbon Number Concept. *J. Chromatogr. Sci.* **1985**, *23*, 333−340.
(33) Issariyakul, T.; Dalai, A. K. Biodiesel from Vegetable Oils. *Renewable Sustainable Energy Rev.* **2014**, *31*, 446−471.
(34) Capella, P.; Zorzut, C. M. Determination of Double Bond Position in Monounsaturated Fatty Acid Esters by Mass Spectrometry of Their Trimethylsilyloxy Derivatives. *Anal. Chem.* **1968**, *40*, 1458−1463, DOI: 10.1021/ac60266a013.
(35) Halket, J. M.; Zaikin, V. G. Derivatization in Mass Spectrometry — 1. Silylation. *Eur. J. Mass Spectrom.* **2003**, *21*, 1−21.
(36) Zaikin, V. G.; Halket, J. M. Derivatization in Mass Spectrometry — 4. Formation of Cyclic Derivatives. *Eur. J. Mass Spectrom.* **2004**, *568*, 555−568.
(37) Mccloskey, J. A.; Mcclelland, M. J. Mass Spectra of 0-Isopropylidene Derivatives of Unsaturated Fatty Esters. *J. Am. Chem. Soc.* **1965**, *10*, 5090−5093.
(38) Pfaendtner, J.; Broadbelt, L. J. Mechanistic Modeling of Lubricant Degradation. 2. The Autoxidation of Decane and Octane. *Ind. Eng. Chem. Res.* **2008**, *47* (9), 2897−2904.
(39) Blanksby, S. J.; Ellison, G. B. Bond Dissociation Energies of Organic Molecules. *Acc. Chem. Res.* **2003**, *36* (4), 255−263.
(40) Frankel, E. N. Chemistry of Free Radical and Singlet Oxidation of Lipids. *Prog. Lipid Res.* **1984**, *23* (4), 197−221.
(41) Jensen, R. K.; Korcek, S.; Zinbo, M. Liquid-Phase Autoxidation of Organic Compounds at Elevated Temperatures. Absolute Rate Constant for Intermolecular Hydrogen Abstraction in Hexadecane Autoxidation at 120−190°C. *Int. J. Chem. Kinet.* **1994**, *26* (6), 673−680.
(42) Jensen, R. K.; Korcek, S.; Zinbo, M.; Johnson, M. D. Initiation in Hydrocarbon Autoxidation at Elevated Temperatures. *Int. J. Chem. Kinet.* **1990**, *22* (10), 1095−1107.
(43) Frankel, E. N. Volatile Lipid Oxidation Products. *Prog. Lipid Res.* **1983**, *22* (1), 1−33.
(44) Knox, J. H. A New Mechanism for the Low Temperature Oxidation of Hydrocarbons in the Gas Phase. *Combust. Flame* **1965**, *9* (3), 297−310.
(45) Stark, M. S.; Waddington, D. J. Oxidation of Propene in the Gas Phase. *Int. J. Chem. Kinet.* **1995**, *27* (2), 123−151.
(46) Ray, D. J. M.; Redfearn, A.; Waddington, D. J. Gas-Phase Oxidation of Alkenes: Decomposition of Hydroxy-Substituted Peroxyl Radicals. *J. Chem. Soc., Perkin Trans. 2* **1973**, *94* (5), 540.
(47) Hammond, C. J.; Lindsay Smith, J. R.; Nagatomi, E.; Stark, M. S.; Waddington, D. J. A Mechanistic Study of the Liquid Phase Autoxidation of Nonan-5-One. *New J. Chem.* **2006**, *30* (5), 741.

DOI: 10.1021/acs.iecr.9b02780
Ind. Eng. Chem. Res. XXXX, XXX, XXX−XXX